Computational Implementation of a Novel Constitutive Model for Multidirectional Composites

G.M. Vyas[a,*], S.T. Pinho[a]

[a]*Department of Aeronautics, Imperial College London, Prince Consort Road, South Kensington, London SW7 2AZ, UK.*

Abstract

This paper details the numerical implementation of a constitutive model for unidirectional (UD) polymer-matrix fibre-reinforced composites, which is able to accurately represent the full non-linear mechanical response. Features such as hydrostatic pressure sensitivity, the effect of multiaxial loading and the dependence of the yield stress on the applied pressure are often neglected in constitutive modelling, but are included in this model.

The constitutive model includes a novel yield function, non-associative flow rule and a non-linear kinematic hardening rule. It is combined with suitable failure criteria and associated damage model. The complete model is implemented in an explicit finite element code.

Experimental test data is used to show that the model is able to predict the non-linear response of both unidirectional and multidirectional composite laminates. The model is shown to accurately predict the constitutive response under complex multiaxial loading and unloading, including significant hydrostatic pressure. Predictions are also shown to compare favourably for the evolution of matrix cracking after ini-

*Corresponding author. Tel: +44 (0)20 7594 5119.
Email address: gv04@imperial.ac.uk (G.M. Vyas)

tial matrix cracking is detected by the failure criteria.

Keywords: Unidirectional Composites, Constitutive Model, Kinematic Hardening, Explicit Integration

1. Introduction

1.1. Background

In recent years the use of fibre-reinforced composites with unidirectional plies has increased, to the extent that primary structural parts in aerospace can now be made using these materials. As a result, the ability to predict exactly when and how these materials will fail is vital. However, if the stress state in the material is not accurately represented, then precise failure predictions are no longer possible.

When considering both unidirectional and multidirectional laminates, an accurate representation of the constitutive response of the material under a variety of uniaxial and combined loading conditions is a necessity for accurate failure predictions and subsequent damage modelling. As well as correctly representing the constitutive response, reliable failure criteria and damage models are then essential for predicting failure **(author?)** [1, 2, 3].

1.2. Important features in the constitutive response of UD composites

The constitutive response in UD composites is complex. Figure 1 shows that the shear response in particular is highly non-linear. This non-linearity – often neglected in the literature – must be taken into consideration when modelling the material response in order to maintain accuracy.

Hydrostatic pressure can cause significantly greater changes in the mechanical properties of polymers and polymer-matrix composites than in metals or rocks, see

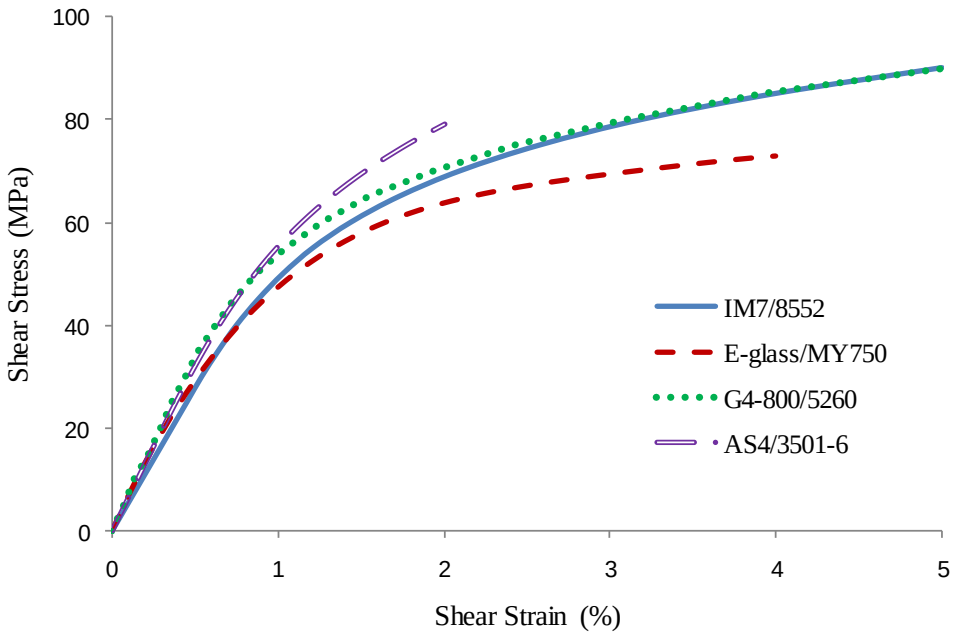
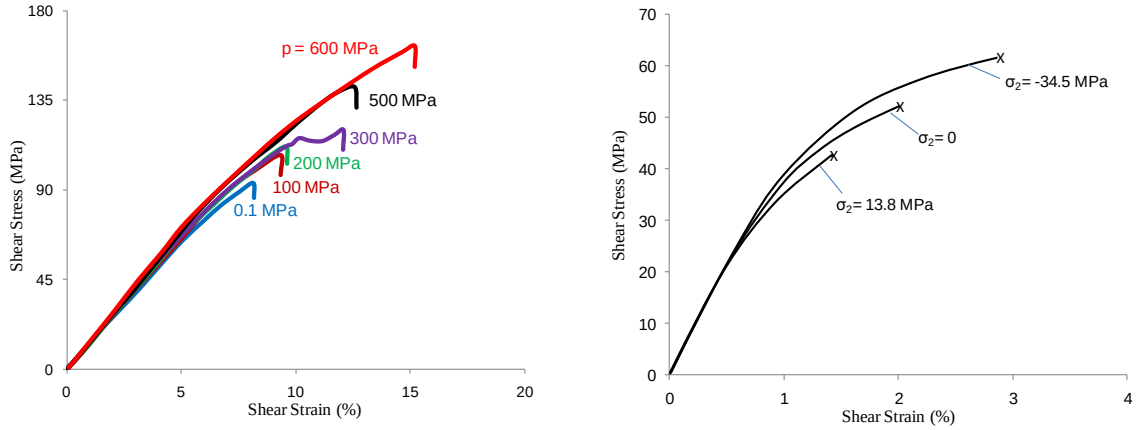


Figure 1: Non-linear shear stress vs. strain response for various UD composites **(author?)** [4, 5]

figure 2a. Furthermore, polymers and polymer-matrix composites yield at different stresses in tension and compression, while the elastic modulus increases with hydrostatic pressure **(author?)** [6, 7, 8].

The presence of fibres in composites materials alters the material dependence on hydrostatic pressure, but the effect is still significant. Pressure increases interfacial normal and shear stresses, resulting in greater adhesion between fibres and matrix, whilst reducing the influence of flaws such as microcracks and voids **(author?)** [7]. The effects of hydrostatic pressure on the non-linear response of a UD composite are shown in figure 2a, indicating an increase in elastic modulus and a change in the behaviour past the point at which non-linearity can be considered significant.



(a) (b)

Figure 2: (a) Effect of increasing hydrostatic pressure on shear response of a UD composite **(author?)** [3, 8] and (b) Effect of multiaxial loading on shear response **(author?)** [9]

Another significant effect is the interaction between different stress components under multiaxial loading, as this also affects the material response. Figure 2b shows that the constitutive response for different stress components is coupled, as the shear response of a UD composite is influenced by the introduction of a stress in the transverse direction.

The following section provides a brief description of the constitutive model used in the paper, which is further detailed in Vyas et al. **(author?)** [10].

2. Overview of Constitutive Model

2.1. Yield Criterion

The proposed yield criterion for unidirectional composites is based on the Raghava criterion for isotropic materials **(author?)** [11], but is generalised to include the hydrostatic sensitivity, μ and the yield stress, σ_0, instead of just the tensile and compressive yield strengths:

$$f = \sqrt{\frac{1}{6}(\sigma_{22} - \sigma_{33})^2 + \sigma_{12}^2 + N\sigma_{23}^2 + \sigma_{31}^2 + \frac{\mu}{2}(\sigma_{22} + \sigma_{33})} - \sigma_0 \qquad (1)$$

Table 1: Definitions of μ and σ_0 using data from different loading tests

Uniaxial test data	μ (MPa)	σ_0 (MPa)
Shear and Compression	$\frac{C}{3} - \frac{2S^2}{C}$	S
Shear and Tension	$\frac{T}{3} + \frac{2S^2}{T}$	S
Tension and Compression	$\frac{C-T}{3}$	$\sqrt{\frac{TC}{6}}$

The constants μ and σ_0 in Equation 1 are calculated using experimental data from any two uniaxial tests, as shown in Table 1, where S is the shear yield stress, T is the yield stress in tension and C is the yield stress in compression. The constant N is included to account for the difference in matrix-dominated shear properties and it can be assumed $N = 1$ **(author?)** [10].

2.2. Flow Rule and Effective Stress

The plastic potential for the flow rule used is defined based on the yield criterion, altering the hydrostatic sensitivity when plastic flow occurs to μ':

$$g = \sqrt{\frac{1}{6}\left(\sigma_{22} - \sigma_{33}\right)^2 + \sigma_{12}^2 + N\sigma_{23}^2 + \sigma_{31}^2 + \frac{\mu'}{2}\left(\sigma_{22} + \sigma_{33}\right)} \tag{2}$$

There are several methods available for the calculation of the value of μ' **(author?)** [10]. In this study, μ' is determined by matching experimental curves from two different uniaxial tests, for example shear and compression, using the effective stress, σ_e.

The effective stress, σ_e, as commonly used in the literature **(author?)** [12], is stated as:

$$\sigma_e = \sqrt{3} f \tag{3}$$

The incremental effective plastic strain, $\mathrm{d}\varepsilon_e^p$, is defined as:

$$\mathrm{d}\varepsilon_e^p = \sqrt{\frac{2}{3}\mathrm{d}\boldsymbol{\varepsilon}_p : \mathrm{d}\boldsymbol{\varepsilon}_p} \tag{4}$$

where $\mathrm{d}\boldsymbol{\varepsilon}_p$ is the incremental plastic strain given by the flow rule **(author?)** [10].

2.3. Hardening Law

Kinematic hardening is included in the model using the back stress, $\boldsymbol{\alpha}$. Kinematic hardening is implemented as it allows for the reproduction of the experimentally observed constitutive behaviour of polymers and unidirectional composites **(author?)** [13, 14] without the need for isotropic hardening. It is also able to model material unloading. From equation 1, the yield criterion then becomes:

$$f = \sqrt{\frac{1}{6}\left(\xi_{22} - \xi_{33}\right)^2 + \xi_{12}^2 + N\xi_{23}^2 + \xi_{31}^2 + \frac{\mu}{2}\left(\sigma_{22} + \sigma_{33}\right)} - \sigma_0 \tag{5}$$

where $\xi_{ij} = \sigma_{ij} - \alpha_{ij}$. The evolution of the back stress is given through the use of the Armstrong-Frederick non-linear kinematic hardening rule **(author?)** [15, 16, 17]:

$$\mathrm{d}\boldsymbol{\alpha} = \frac{2}{3}c\mathrm{d}\boldsymbol{\varepsilon}_p - \gamma\boldsymbol{\alpha}\mathrm{d}\varepsilon_e^p \tag{6}$$

where c is a material constant, γ is a material variable which depends on hydrostatic pressure – as detailed in section 2.4 – and $\mathrm{d}\boldsymbol{\alpha}$ is the increment in back stress.

2.4. Pressure Dependence

Previous studies have indicated the elastic modulus of polymers and composites is greater when hydrostatic pressure is applied **(author?)** [8, 18]. The effect of hydrostatic pressure in the elastic region is modelled by assuming a linear increase in Young's modulus and shear modulus, E and G respectively, with hydrostatic pressure **(author?)** [3]:

$$E = E_0 + \eta_E\sigma_m \tag{7}$$

$$G = G_0 + \eta_G\sigma_m \tag{8}$$

where E_0 and G_0 are the Young's and shear moduli with no applied hydrostatic pressure and η_E and η_G are the slope coefficients for the secant Young's and shear modulus, respectively. As the fibre direction is not affected by this increase due to the presence of fibres, here σ_m is defined as:

$$\sigma_m = \frac{1}{2}(\sigma_{22} + \sigma_{33}) \tag{9}$$

To model the modulus change with hydrostatic pressure in the non-linear region (see figure 2a), an exponential evolution of γ in equation 6 is used:

$$\gamma = \gamma^0 e^{\eta_\gamma \sigma_m} \tag{10}$$

where γ^0 is the initial value of γ. The value of the slope coefficient for γ, η_γ, is defined based on experimental observations of the evolution of γ with increasing pressure.

3. Combination with failure criteria and damage model

3.1. Constitutive Model Algorithm

The model has been coded as both an independent subroutine in Abaqus/Explicit (VUMAT) and as a complete subroutine, with the failure criteria and associated continuum damage model described by Pinho et al. **(author?)** [3].

An explicit implementation is utilised to overcome the convergence difficulties associated with implicit implementations **(author?)** [19]. The algorithm for the constitutive model for explicit integration is shown in figure 3. The algorithm follows a general return algorithm with an elastic predictor – as described by Simo and Hughes **(author?)** [20] – and due to the explicit formulation the forward Euler method is used **(author?)** [21].

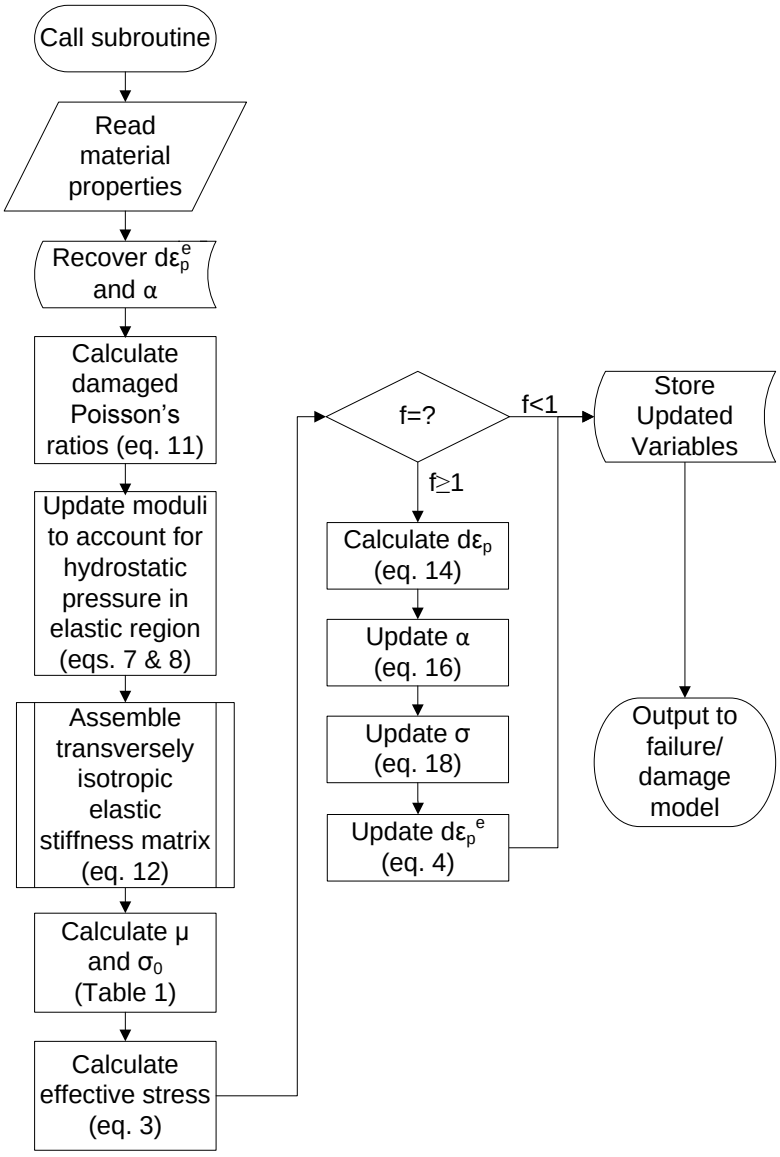


Figure 3: Algorithm for Abaqus/Explicit VUMAT subroutine

3.1.1. Damaged Poisson's Ratio

At any increment, the Poisson's ratio, ν_{ab}, is modified to account for existing damage, using the available damage variable from the previous increment:

$$\nu_{ab}^{dam} = (1 - d_{max})\,\nu_{ab} \tag{11}$$

where d_{max} is the maximum value of the damage variable, accounting for the four failure modes considered, which will be detailed in section 3.2.1.

3.1.2. Stiffness matrix calculation

The stiffness matrix follows Hooke's Law for orthotropic materials. In flexibility form, this is:

$$\begin{bmatrix} \varepsilon_1 \\ \varepsilon_2 \\ \varepsilon_3 \\ \gamma_{23} \\ \gamma_{31} \\ \gamma_{12} \end{bmatrix} = \begin{bmatrix} \frac{1}{E_1} & \frac{-\nu_{12}}{E_1} & \frac{-\nu_{13}}{E_1} & 0 & 0 & 0 \\ \frac{-\nu_{21}}{E_2} & \frac{1}{E_2} & \frac{-\nu_{23}}{E_2} & 0 & 0 & 0 \\ \frac{-\nu_{31}}{E_3} & \frac{-\nu_{32}}{E_3} & \frac{1}{E_3} & 0 & 0 & 0 \\ 0 & 0 & 0 & \frac{1}{G_{23}} & 0 & 0 \\ 0 & 0 & 0 & 0 & \frac{1}{G_{31}} & 0 \\ 0 & 0 & 0 & 0 & 0 & \frac{1}{G_{12}} \end{bmatrix} \begin{bmatrix} \sigma_1 \\ \sigma_2 \\ \sigma_3 \\ \tau_{23} \\ \tau_{31} \\ \tau_{12} \end{bmatrix} \tag{12}$$

$$\boldsymbol{\varepsilon} = \mathbf{D}_e^{-1}\boldsymbol{\sigma} \tag{13}$$

with the subscript 1 denoting the fibre direction, 2 the in-plane transverse direction and 3 the through-the-thickness direction.

Assuming transverse isotropy, equation 12 can be further simplified, as $E_3 = E_2$, $G_{13} = G_{12}$, $\nu_{13} = \nu_{12}$ and $G_{23} = \frac{E_2}{2(1+\nu_{23})}$.

3.1.3. Calculation of the plastic multiplier

The incremental plastic strain, $\mathrm{d}\boldsymbol{\varepsilon}_p$ is calculated using the flow rule:

$$\mathrm{d}\boldsymbol{\varepsilon}_p = \mathrm{d}\lambda \frac{\partial g}{\partial \boldsymbol{\sigma}} \tag{14}$$

where $\mathrm{d}\lambda$ is the plastic multiplier. The full derivation of the plastic multiplier follows Dunne and Petrinic **(author?)** [16] for an associative flow plastic multiplier. For non-associative flow, this leads to:

$$\mathrm{d}\lambda = \frac{f_\sigma \mathbf{D}_e \mathrm{d}\boldsymbol{\varepsilon}}{f_\sigma \mathbf{D}_e g_\sigma + \gamma f_\alpha \boldsymbol{\alpha} - \left(\frac{2}{3}\right) c f_\alpha g_\sigma} \tag{15}$$

where $f_\sigma = \frac{df}{d\boldsymbol{\sigma}}$, $f_\alpha = \frac{df}{d\boldsymbol{\alpha}}$, $g_\sigma = \frac{dg}{d\boldsymbol{\sigma}}$ and $\mathbf{D}_e$ is the elastic stiffness matrix.

3.1.4. Updating back stress, stress and effective plastic strain

The back stress is updated using the incremental back stress shown in equation 6. The back stress is then:

$$\boldsymbol{\alpha}_{new} = \boldsymbol{\alpha}_{old} + \mathrm{d}\boldsymbol{\alpha} \tag{16}$$

The back stress, $\boldsymbol{\alpha}$ can be used with equation 5 to determine the value of the yield function, f_{new}. If $f_{new} < 1$ then the yield surface has not been exceeded and the updated stress, $\boldsymbol{\sigma}_{new}$, is calculated directly from the constitutive law in equation 12. If $f_{new} \geq 1$ then the yield surface has been exceeded and the updated stress is calculated as:

$$\mathrm{d}\boldsymbol{\sigma}_{new} = \mathbf{D}_e \mathrm{d}\boldsymbol{\varepsilon} + \mathrm{d}\boldsymbol{\alpha} \tag{17}$$

$$\boldsymbol{\sigma}_{new} = \boldsymbol{\sigma}_{old} + \mathrm{d}\boldsymbol{\sigma}_{new} \tag{18}$$

where $\mathrm{d}\boldsymbol{\alpha}$ is the increment in back stress given in equation 18.

The effective plastic strain is calculated as shown in equation 4.

3.2. Complete constitutive, failure and damage model

3.2.1. Failure Onset Indices

The failure criteria are taken from Pinho et al. **(author?)** [3] and include failure indices for fibre failure, matrix failure, fibre kinking and fibre splitting.

The failure index for matrix failure is a modified version of the Mohr-Coulomb criterion adapted for UD composites:

$$FI_M = \left(\frac{\tau_T}{S_T^{is} - \eta_T \sigma_N}\right)^2 + \left(\frac{\tau_L}{S_L^{is} - \eta_L \sigma_N}\right)^2 + \left(\frac{\langle \sigma_N \rangle_+}{Y_T^{is}}\right)^2 \tag{19}$$

where τ_T and τ_L are the transverse and longitudinal shear component of the traction, Y_T^{is} is the in-situ in-plane transverse tensile shear strength, S_T^{is} and S_L^{is} are the transverse and longitudinal in-situ transverse shear strengths. σ_N is the normal component of the traction and η_T and η_L are the slope coefficients for transverse and longitudinal shear strength, respectively.

The failure index for fibre tensile failure is based on a maximum stress criterion and is stated as:

$$FI_{FT} = \frac{\langle \sigma_N \rangle_+}{X_T} \tag{20}$$

where X_T is the longitudinal tensile strength.

For fibre kinking and splitting failure, the same failure index is used:

$$FI_{KINK} = FI_{SPLIT} = \left(\frac{\tau_{2^m 3^\psi}}{S_T^{is} - \eta_T \sigma_{2^m}}\right)^2 + \left(\frac{\tau_{1^m 2^m}}{S_L^{is} - \eta_L \sigma_{2^m}}\right)^2 + \left(\frac{\langle \sigma_{2^m} \rangle_+}{Y_T^{is}}\right)^2 \tag{21}$$

Fibre kinking is predicted if $\sigma_1 \leq -\frac{X_C}{2}$ and fibre splitting is occurring if $\sigma_1 \geq -\frac{X_C}{2}$, where X_C is the longitudinal compressive strength. ψ denotes the angle of the kink band and is found numerically so as to maximise FI_{KINK}. The superscript m denotes a coordinate system aligned with an initial misalignment angle, detailed by Pinho et al. **(author?)** [3, 22, 23].

3.2.2. Damage Model

Once failure is predicted by any of equations 19-21, the traction acting on the fracture plane is reduced to zero, using a cohesive zone in such a way that the correct fracture toughness for the specific failure mode is attained, as by Pinho et al. **(author?)** [3]. For matrix cracking in multidirectional laminates, a constant stress is assumed during the accumulation of cracks, and the traction components are only reduced to zero when delamination is predicted to occur using a shear lag model **(author?)** [22, 23], as shown in figure 4. The strains ε^o, ε^d and ε^f indicate cracking onset, delamination onset and the strain at complete decohehsion, respectively . This model for matrix cracking has been compared against other models in the literature by Schuecker et al. **(author?)** [24] and was shown to compare particularly well.

The maximum damage variable for degrading the Poisson's ratios (equation 11), d_{max}, is defined as:

$$d_{max} = max\left(d_{ft},\, d_{kink},\, d_{split},\, d_{mat}\right) \tag{22}$$

and the subscripts ft, $kink$, $split$ and mat represent fibre tension, kinking, splitting and matrix damage, respectively.

The energy per unit volume dissipated by the formation of cracks in a ply embedded within the lamina is $U_{crack} = \frac{1}{2}\sigma^0\left(\varepsilon^d - \varepsilon^0\right)$, as shown in figure 4. The strain at the onset of delamination is given by:

$$\varepsilon^d = \varepsilon^0 + \frac{2nG_c}{\sigma^0} \tag{23}$$

where G_c is the critical energy release rate for the failure mode, n is the saturation crack density and σ^0 is the magnitude of the traction at the onset of failure. Further

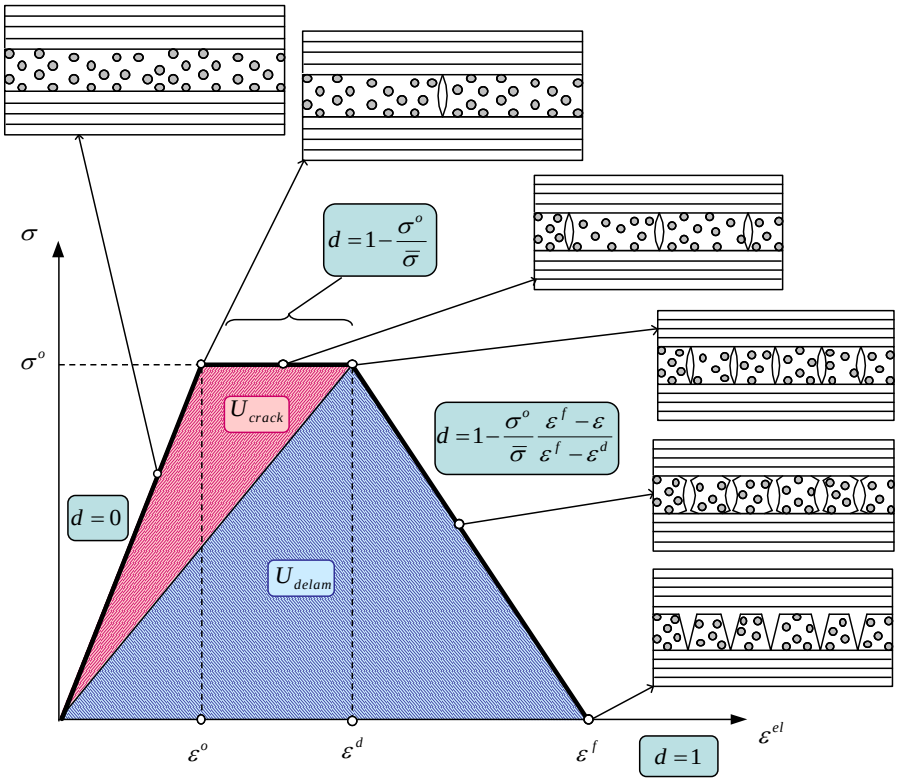


Figure 4: Progressive cracking for a ply in a multidirectional laminate **(author?)** [3]

loading beyond ε^d will result in delamination, where the energy dissipated by the model is $U_{delam} = \frac{1}{2}\sigma^0\varepsilon^f$.

To reproduce the stress-strain response shown in figure 4, the damage variable, d, is defined as the maximum value in time of

$$d^{inst} = \max\left\{0,\ \min\left\{1 - \frac{\sigma^0}{\bar{\sigma}},\ 1 - \frac{\sigma^0}{\bar{\sigma}}\frac{\varepsilon^f - \varepsilon}{\varepsilon^f - \varepsilon^d},\ 1\right\}\right\} \tag{24}$$

$$d = \max_{time}\left\{d^{inst}\right\} \tag{25}$$

where $\bar{\sigma}$ is the magnitude of the effective traction vector.

3.2.3. Complete Model Algorithm

The algorithm for the complete constitutive, failure and damage model is shown in figure 5. The current stress state is computed using the constitutive model. The failure criteria are then applied to determine whether failure has occurred using the stress state from the constitutive model. If failure has occurred, the material properties are degraded accordingly by the damage model. The updated variables are then stored for the next increment and output back to the FE code.

4. Applications

The constitutive law, failure criteria and damage model (hereby termed the 'complete' model) is applied to simulate the constitutive response and the matrix crack accumulation of several laminates found in the literature. Furthermore, the implementation is tested in the simulation of unloading and predictions are made for the modulus drop of a laminate. All predictions are made using a simple model of the laminate with appropriate boundary conditions. One element per ply is used, with reduced integration 3D brick elements.

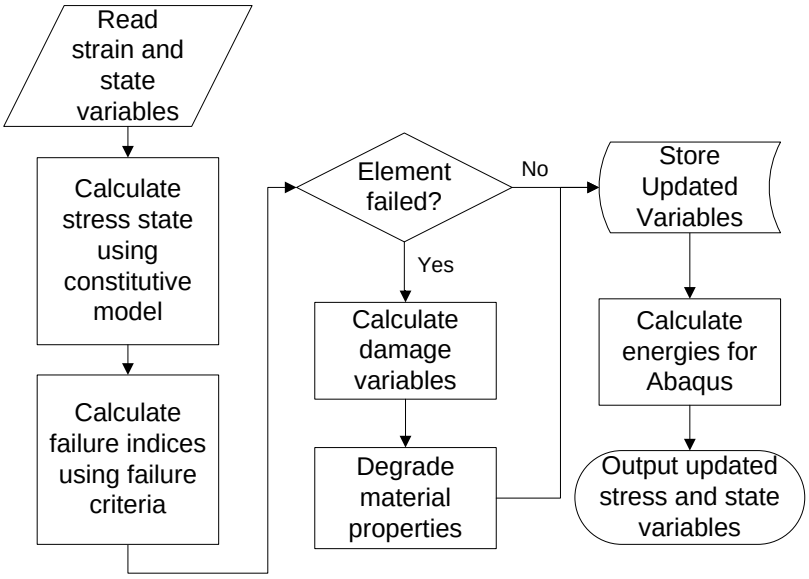


Figure 5: Algorithm for complete constitutive, failure and damage model

The input data used is shown in Table 2, in which the elastic properties and strengths are found in the literature **(author?)** [5, 25]. The in-situ values are calculated following a previously outlined shear lag based approach **(author?)** [1, 2, 3]. The determination of the parameters for the constitutive model have been outlined by the authors in a previous work **(author?)** [10], with the compressive and shear yield stresses, C and S, respectively, being measured as the onset of non-linearity in experimental stress-strain curves given by Kaddour et al. **(author?)** [5]. γ^0 is calculated by plotting the non-linear hardening law with no applied hydrostatic pressure and comparing with the constitutive response curves.

In order to compare the developed model with a simpler third order polynomial extrapolation, experimental data for the shear and transverse compressive response of E-glass/MY750 is required. This is shown in figure 6, from which the coefficients of the third order polynomials are obtained.

Table 2: Material properties used for predictions

	E-Glass/MY750 [5]	HyE 9082Af/Fiberite [25]	IM7/8552 [5]
Longitudinal modulus, E_1 (GPa)	45.6	44.7	165
Transverse modulus, E_2 (GPa)	16.2	12.7	9
Shear Modulus, G_{12} (GPa)	5.8	5.8	5.6
In-plane shear modulus, ν_{12}	0.278	0.297	0.34
Longitudinal tensile strength, X_T (MPa)	1280	$1280^{\triangle}$	2560
Longitudinal compressive strength, X_C (MPa)	800	$800^{\triangle}$	1590
Transverse tensile strength, Y_T (MPa)	40	$40^{\triangle}$	73
Transverse compressive strength, Y_C (MPa)	145	$145^{\triangle}$	185
In-plane shear strength, S_L (MPa)	73	$73^{\triangle}$	90
Hardening law material constant, c	70 000	80 000	100 000
Initial value of γ in hardening law, γ^0	100	110	60
Slope coefficient for γ, η_γ	$0.002^{\dagger}$	$0.002^{\dagger}$	$0.002^{\dagger}$
Compressive yield stress, C (MPa)	90	$90^{\triangle}$	122
Shear yield stress, S (MPa)	34	$34^{\triangle}$	52
Slope coefficient for Young's modulus, η_G	$0.2^{\dagger}$	$0.2^{\dagger}$	$0.2^{\dagger}$
Slope coefficient for shear modulus, η_E	$16^{\dagger}$	$16^{\dagger}$	$16^{\dagger}$
In-situ transverse tensile strength, Y_T^{is} (MPa)	113	$113^{\triangle}$	89
In-situ transverse shear strength, S_T^{is} (MPa)	114	$114^{\triangle}$	81
In-situ longitudinal shear strength, S_L^{is} (MPa)	87	$87^{\triangle}$	93
Transverse shear strength slope coefficient, η_T	0.287*	0.287*	0.287*
Longitudinal shear strength slope coefficient, η_L	0.082*	0.082*	0.082*

*estimated values based on authors' experience and literature [3]
†calculated from the experimental curves of Shin and Pae [8] with an exponential evolution of γ
$^{\triangle}$Assumed values based on a similar material (E-Glass/MY750)

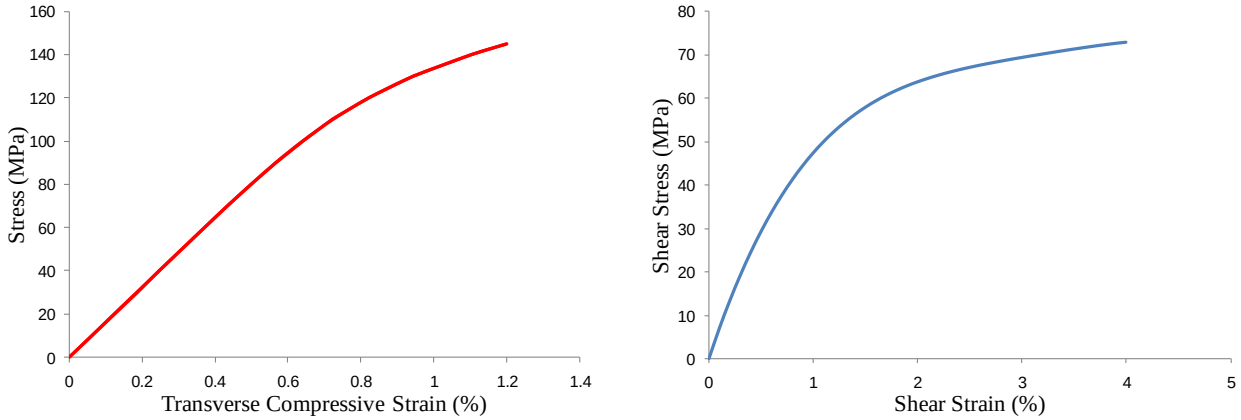


Figure 6: Experimental curves of a) transverse compressive and b) shear response of E-Glass/MY750 **(author?)** [5]

4.1. Stress vs. strain and crack accumulation

A $(0°/90_n°)_s$ E-glass/MY750 laminate loaded in tension in the fibre direction of the 0° plies is simulated using the complete model. Each ply has a thickness of 0.125 mm and predictions are made up to fibre fracture in the 0° plies. Figure 7 shows the predicted stress vs. strain curves and crack density variation using a) a simple third order polynomial extrapolation of the experimental constitutive data (shown in figure 6) and b) the new constitutive model. The experimental data shown is for a similar material tested by Joffe and Varna **(author?)** [26], with a ply thickness of 0.144 mm.

Similarly, a quasi-isotropic laminate of the same material is simulated and compared with experimental data from Tong et al. **(author?)** [27]. The layup is $(0°/90°/-45°/+45°)_s$, the ply thickness is 0.5 mm and the loading is in the direction of the 0° plies. Again, the prediction is shown up to fibre fracture in the 0° plies in figure 8a) using an existing linear constitutive model and figure 8b) using the new constitutive model based on plasticity theory.

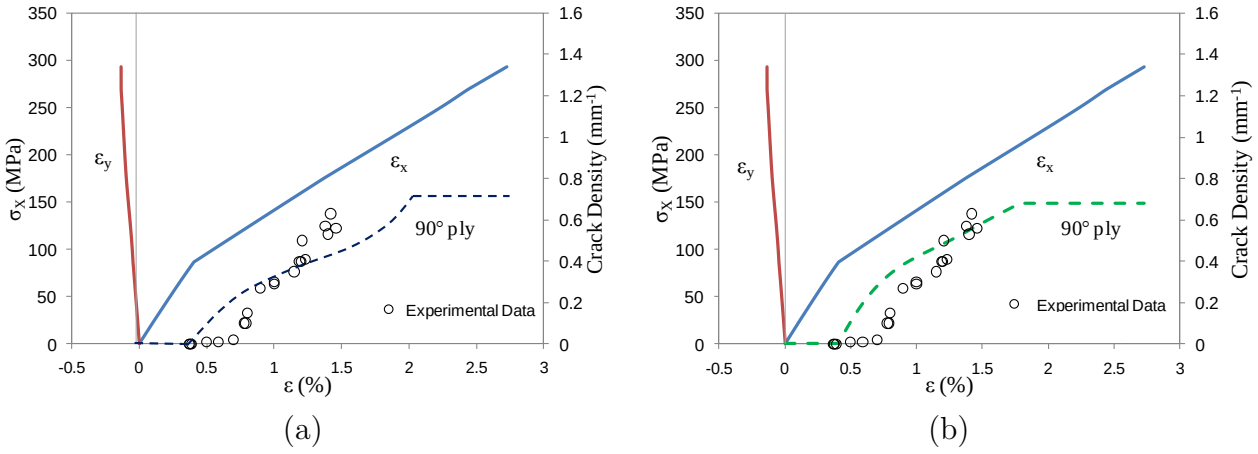


Figure 7: Predicted stress vs. strain response and crack density variation for a $(0°/90_n°)_s$ laminate of E-glass/MY750 with (a) polynomial extrapolation and (b) new constitutive model. Experimental crack density results are taken from Joffe and Varna **(author?)** [26]

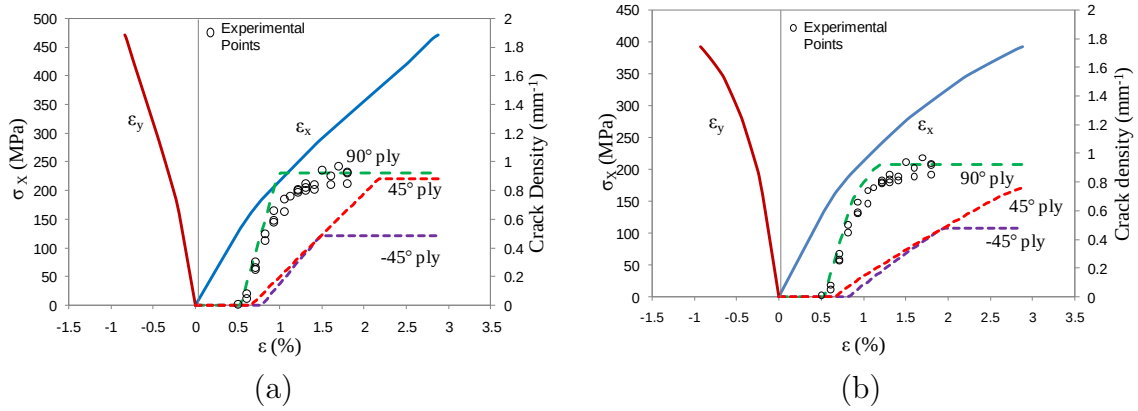


Figure 8: Predicted stress vs. strain response and crack density variation for a $(0°/90°/-45°/+45°)_s$ laminate of E-glass/MY750 using a) existing linear constitutive model and b) new constitutive model. Experimental data from Tong et al. **(author?)** [27]

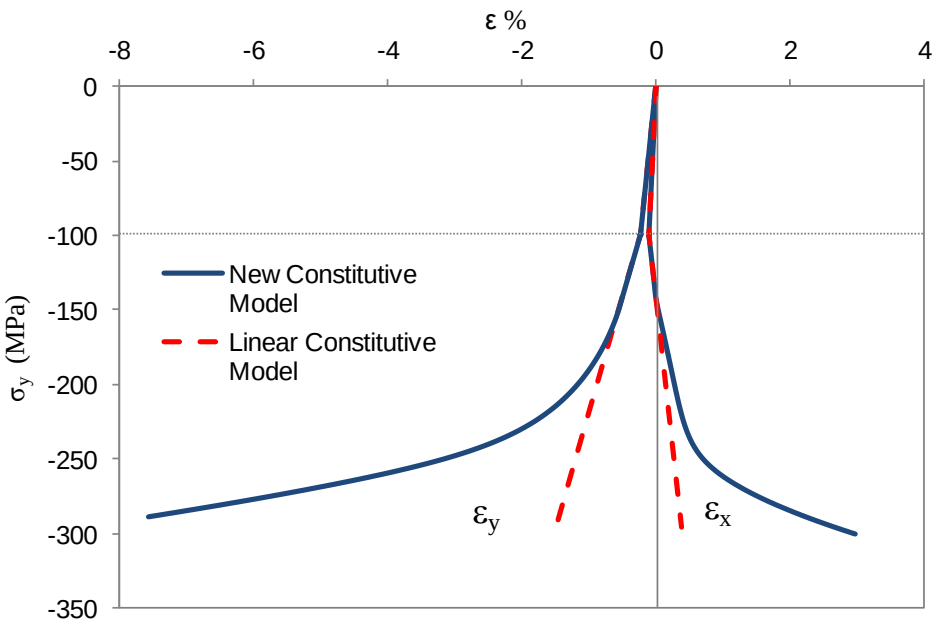


Figure 9: Predicted stress vs. strain response for a $\pm 35°$ laminate of E-glass/MY750 with $\sigma_x = \sigma_z = -100$ MPa

4.2. Stress-strain response with hydrostatic pressure

A $\pm 35°$ laminate of E-glass/MY750 is compressively loaded in the y-direction with a superimposed hydrostatic pressure of $\sigma_x = \sigma_z = -100$ MPa. The ply thickness of the laminate is 0.25 mm. Figure 9 shows the predicted response using the complete model and a linear constitutive model.

4.3. Modelling of unloading

To test the modelling of unloading, the stand-alone VUMAT is used for a single $90°$ ply of IM7/8552 with 0.5 mm ply thickness. A load of 180 MPa is applied transverse to the fibres, then removed, before the material is reloaded to 200 MPa. The simulated response is shown in figure 10.

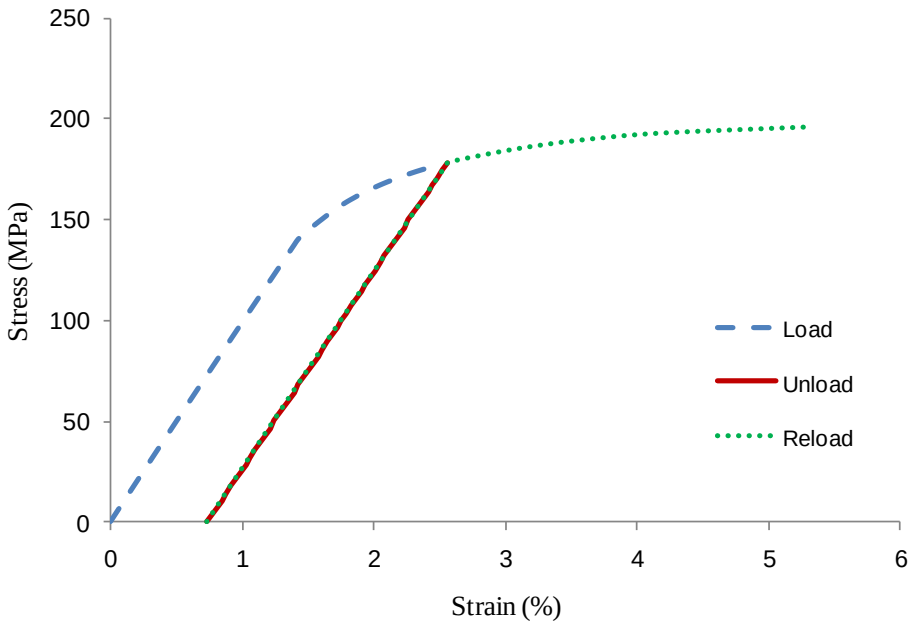


Figure 10: Simulation of applied compressive loading, unloading and reloading of a single 90° ply of IM7/8552

4.4. Predicted modulus change

The complete model has also been used to predict the change in modulus of a HYE 9082Af/Fiberite laminate with a $(0°/\pm 40_4°/0_{\frac{1}{2}}°)_s$ layup under an axial loading. As the ply thickness is not given in the literature, it is assumed to be 0.144 mm, based on a similar material **(author?)** [5]. The result of the simulation is plotted with the experimental data for two specimens taken from Varna et al. **(author?)** [25], shown in figure 11.

5. Discussion

The examples shown in the previous section demonstrate that the complete constitutive law, failure criteria and damage model is capable of accurately predicting the response of UD composite materials.

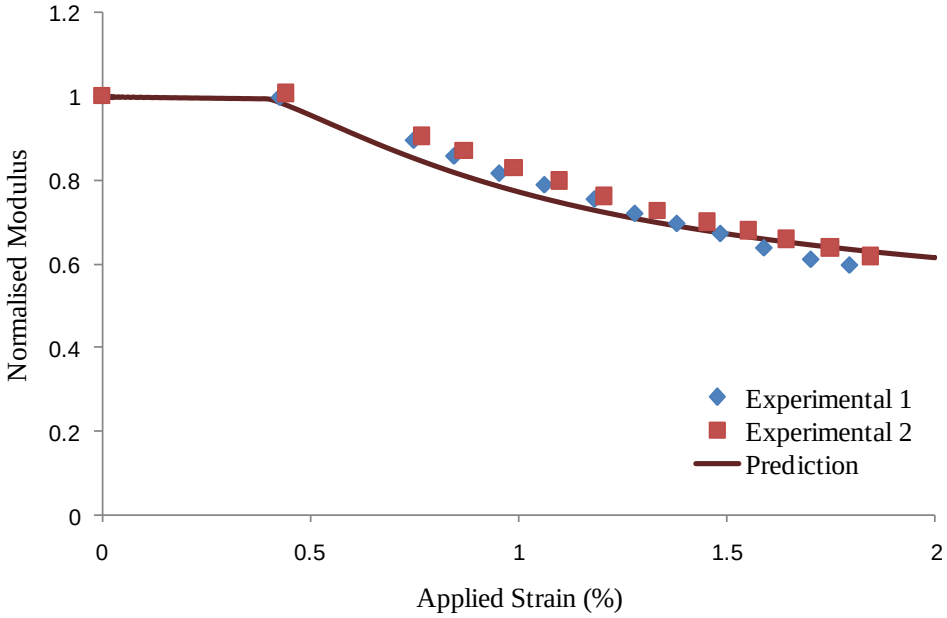


Figure 11: Predicted normalised modulus with increasing strain for a $(0°/\pm 40_4°/0_{\frac{1}{2}}°)_s$ HyE 9082Af/Fiberite laminate. Experimental data from Varna et al. **(author?)** [25]

The complete model is able to predict the crack density variation for a cross-ply laminate displays a reasonable fit to the experimental data, as shown in figure 7b) . The constitutive response is similar regardless of which type of extrapolation (simple third order polynomial or new constitutive model) is used, as the response of the $(0°/90_n°)_s$ laminate is dominated by the ratio of 0° to $90_n°$ plies. The observed "knee" in the results is typical of this layup **(author?)** [28, 29]. However, a significant difference is seen between the two types of extrapolation in the prediction of the crack density evolution, with the new model predicting a more physically sensible curve than the polynomial extrapolation up to the saturation value.

The predicted crack density for quasi-isotropic E-glass/MY750 laminates closely matches the experimental data from Tong et al. **(author?)** [27] using the new constitutive model. This is shown in figure 8b), which again (as with figure 9) shows

the non-linearity produced by the model in the prediction of the constitutive response. Figure 8a) indicates that the crack accumulation prediction made using a linear constitutive model does not capture the crack accumulation as well as the plasticity based constitutive model. The change in the predicted constitutive response between a linear continuum damage model and the new complete model is clearly visible in figure 9.

The constitutive model is able to satisfactorily simulate material unloading at the current modulus, followed by reloading (figure 10). This simulation is often overlooked when using several other extrapolation methods found in the literature for the modelling of UD composites, but is included in the present model through the use of the non-linear kinematic hardening law.

The experimentally observed modulus drop is predicted in excellent agreement with the published results **(author?)** [25], as demonstrated in figure 11. This prediction requires the experimental curves and ply thickness to be known. As not all of the necessary material properties were available, some properties were assumed based on a similar material (E-glass/MY750), but the prediction made still matches the experimental results very well.

6. Conclusions

An improved constitutive model for unidirectional composite materials which accounts for hydrostatic pressure and multiaxial loading effects has been combined with a set of failure criteria and damage model. The complete model is coded as a material subroutine in a commercial finite element code (Abaqus/Explicit VUMAT). Using the new complete constitutive, failure and damage model, predictions are made that closely reproduce the observed experimental behaviour of unidirec-

tional composites with varying layups and ply thicknesses. Furthermore, the effect of material unloading is modelled through the use of kinematic hardening, a factor which is sometimes overlooked when modelling UD composites with continuum damage models.

Acknowledgment

The authors wish to acknowledge the support of the EPSRC and Airbus UK through CASE Award 08000674.

References

[1] C.G. Dávila, P.P. Camanho, and C.A. Rose. Failure criteria for FRP laminates. *Journal of Composite Materials*, 39(4):323, 2005.

[2] S.T. Pinho, C.G. Dávila, P.P. Camanho, L. Iannucci, and P. Robinson. Failure models and criteria for FRP under in-plane or three-dimensional stress states including shear non-linearity. *NASA Technical Memorandum*, 213530, 2005.

[3] S.T. Pinho, R. Darvizeh, P. Robinson, C. Schuecker, and P.P. Camanho. Material and structural response of polymer-matrix fibre-reinforced composites. *Composites Science and Technology*, Accepted for publication:(Special issue on Second World Wide Failure Exercise), 2008.

[4] A.S. Kaddour and M.J. Hinton. Instructions to contributors of the second world-wide failure exercise (WWFE-II): Part (a). 2007.

[5] A.S. Kaddour, M.J. Hinton, S. Li, and P. Smith. Instructions to contributors of the third world-wide failure exercise (WWFE-III): Part (a). 2008.

[6] H. Altenbach and K. Tushtev. A new static failure criterion for isotropic polymers. *Mechanics of Composite Materials*, 37(5):475–482, 2001.

[7] C.P.R. Hoppel, T.A. Bogetti, and J.W. Gillespie. Effects of hydrostatic pressure on the mechanical behavior of composite materials. *Journal of Thermoplastic Composite Materials*, 8:375–375, 1995.

[8] E.S. Shin and K.D. Pae. Effects of hydrostatic pressure on in-plane shear properties of graphite/epoxy composites. *Journal of Composite Materials*, 26(6):828, 1992.

[9] S.R. Swanson, M.J. Messick, and Z. Tian. Failure of carbon/epoxy lamina under combined stress. *Journal of Composite Materials*, 21(7):619, 1987.

[10] GM Vyas, ST Pinho, and P. Robinson. Constitutive modelling of fibre-reinforced composites with unidirectional plies using a plasticity-based approach. *Composites Science and Technology*, 71(8):1068–1074, 2011.

[11] R. Raghava, R.M. Caddell, and G.S.Y. Yeh. The macroscopic yield behaviour of polymers. *Journal of Materials Science*, 8(2):225–232, 1973.

[12] R.K. Goldberg, G.D. Roberts, and A. Gilat. Implementation of an associative flow rule including hydrostatic stress effects into the high strain rate deformation analysis of polymer matrix composites. *Journal of Aerospace Engineering*, 18:18, 2005.

[13] G.Z. Voyiadjis and G. Thiagarajan. An anisotropic yield surface model for directionally reinforced metal-matrix composites. *International Journal of Plasticity*, 11(8):867–894, 1995.

[14] G.J. Dvorak et al. An experimental study of elastic-plastic behavior of a fibrous boron-aluminum composite. *Journal of the Mechanics and Physics of Solids*, 36(6):655–687, 1988.

[15] M. Jirasek. Modeling of localized inelastic deformation. Czech Technical University, 2006.

[16] F. Dunne and N. Petrinic. *Introduction to computational plasticity*. Oxford University Press, USA, 2005.

[17] J. Lubliner. *Plasticity Theory*. Pearson Education, 2006.

[18] P.J. Hine, R.A. Duckett, A.S. Kaddour, M.J. Hinton, and G.M. Wells. The effect of hydrostatic pressure on the mechanical properties of glass fibre/epoxy unidirectional composites. *Composites Part A*, 36(2):279–289, 2005.

[19] F.J. Harewood and P.E. McHugh. Comparison of the implicit and explicit finite element methods using crystal plasticity. *Computational Materials Science*, 39(2):481–494, 2007.

[20] J.C. Simo and T.J.R. Hughes. *Computational Inelasticity*. Springer, 2000.

[21] Abaqus. *Abaqus 6.9 Documentation*. Simulia, 2009.

[22] S.T. Pinho, L. Iannucci, and P. Robinson. Physically based failure models and criteria for laminated fibre-reinforced composites with emphasis on fibre kinking. Part II: FE implementation. *Composites Part A: Applied Science and Manufacturing*, 37(5):766–777, 2006.

[23] S.T. Pinho, P. Robinson, C. Schuecker, and P. Camanho. Pressure-dependent constitutive and failure model for laminated composites. In *Proceedings of the*

17th international conference on composite materials (ICCM17), Edinburgh, Scotland, 2009.

[24] C. Schuecker, C.G. Dávila, and A. Rose. Comparison of damage models for predicting the non-linear response of laminates under matrix dominated loading conditions. *NASA/TP-2010-216856*, 2010.

[25] J. Varna, R. Joffe, N.V. Akshantala, and R. Talreja. Damage in composite laminates with off-axis plies. *Composites Science and Technology*, 59(14):2139–2147, 1999.

[26] R. Joffe and J. Varna. Analytical modeling of stiffness reduction in symmetric and balanced laminates due to cracks in 90 layers. *Composites Science and Technology*, 59(11):1641–1652, 1999.

[27] J. Tong, F.J. Guild, S.L. Ogin, and P.A. Smith. On matrix crack growth in quasi-isotropic laminates - I. Experimental investigation. *Composites Science and Technology*, 57(11):1527–1535, 1997.

[28] K.W. Garrett and J.E. Bailey. Multiple transverse fracture in 90 cross-ply laminates of a glass fibre-reinforced polyester. *Journal of materials science*, 12(1):157–168, 1977.

[29] A. Parvizi, K.W. Garrett, and J.E. Bailey. Constrained cracking in glass fibre-reinforced epoxy cross-ply laminates. *Journal of Materials Science*, 13(1):195–201, 1978.